ICARUS **127,** 290–306 (1997)
ARTICLE NO. IS975712

The Origin of Comets in the Solar Nebula: A Unified Model

S. J. Weidenschilling

Planetary Science Institute/SJI, 620 North Sixth Avenue, Tucson, Arizona 85705-8331
E-mail: sjw@psi.edu

Received November 6, 1996; revised January 31, 1997

Comets originated as icy planetesimals in the outer Solar System, as shown by dynamical studies and direct observation of objects in the Kuiper disk. Their nuclei have low strength consistent with "rubble pile" structure and inhomogeneities on scales of tens to hundreds of meters. These properties can be explained by their formation process in the solar nebula.

I present results of numerical simulation of the growth of cometesimals, beginning with a uniform mixture of microscopic grains in the nebular gas. Coagulation and settling yield a thin, dense layer of small aggregates in the central plane of the nebula. Shear between this layer and the pressure-supported gas produces turbulence that initially inhibits gravitational instability. Particles grow by collisional coagulation; relative velocities are dominated by radial motion due to orbital decay induced by gas drag. The radial velocity dispersion further delays gravitational instability until the mean particle size reaches tens of meters. Lack of damping in the swarm of macroscopic particles limits gravitational instability to large scales that do not allow collapse to solid bodies. Collisional coagulation is responsible for growth even after instability occurs.

The size distribution of cometesimals growing by drag-induced collisions develops a narrow peak in the range tens to hundreds of meters. This occurs because drag-induced velocities decrease with size in this range, while gravitational focusing is negligible. Impact velocities have a minimum at the transition from drag-driven to gravitational accretion at approximately kilometer sizes. Bodies accreted in this manner should have low mechanical strength and macroscopic voids in addition to small-scale porosity. They will be composed of structural elements having a variety of scales, but with some tendency for preferential sizes in the range ~10–100 m. These properties are in good agreement with inferred properties of comets, which may preserve a physical record of their accretion. © 1997 Academic Press

I. INTRODUCTION

Many origins have been suggested for comets. Historically, there has been a dichotomy between theories that regarded them as exotic material captured from interstellar space and those that accepted them as sharing a common origin with the Solar System (cf. Weissman 1985 and references therein). While consensus appeared to favor the latter class of theories, there were many variants: comets formed during collapse of the presolar cloud, in distant subnebulas, or as planetesimals within the solar nebula. In the latter version, comets would be distinct from asteroids only by forming from volatile-rich material at greater heliocentric distances and lower temperatures.

In recent years the preponderance of evidence has favored this last hypothesis: comets are icy planetesimals that formed within the outer reaches of the solar nebula. This conclusion was strongly supported by dynamical studies (Duncan *et al.* 1988) that demonstrated that short-period comets were derived from a transneptunian reservoir of objects in low-inclination orbits, the so-called "Kuiper Belt." The existence of the Kuiper Belt was confirmed by observations of these objects *in situ,* with large (>100 km) bodies observed from the ground (Jewitt and Luu 1995), and smaller ones (~10 km) detected by the Hubble telescope (Cochran *et al.* 1995). There can be little doubt that these objects formed in the outer fringes of the solar nebula and that they are the major source of presently observed short-period comets. By logical extension, the long-period and parabolic comets from the Oort cloud also originated in the solar nebula, but at somewhat smaller heliocentric distances. They were placed into more distant orbits by perturbations of the outer planets (Safronov 1969, Fernandez and Ip 1981).

As distant planetesimals, comets are probably the least-altered (though not necessarily pristine) objects surviving from the origin of the Solar System. As such, they may preserve some record of the processes involved in their formation within the solar nebula. While meteorites contain abundant chemical and isotopic evidence for conditions in the nebula, the record of their accretion has been obscured by aqueous alteration, thermal metamorphism, and (especially) the extensive collisional evolution of the asteroids. While the inner part of the Kuiper disk has probably experienced collisional evolution over the age of the Solar System, this has been less extensive, with lower collision velocities, than in the asteroid belt. The outer part beyond ≃45 AU, if populated at all, has survived with

0019-1035/97 $25.00

little alteration. The inner disk probably supplies most short-period comets. A substantial fraction of kilometer-sized comets may be collisional fragments, but were derived from parent bodies not larger than a few tens of kilometers in size (Farinella and Davis 1996).

As we have no macroscopic samples of cometary material, most properties of cometary nuclei must be derived from remote sensing. It is obvious that comets are not simple structureless aggregates of primordial grains. They display complex temporal and spatial variations (outbursts and jetting). The sizes of outbursts suggest compositional inhomogeneities of scale ~20–100 m (Whitney 1955, Larson *et al.* 1990, Mumma *et al.* 1993), which are ascribed to accretion of kilometer-sized or larger nuclei from smaller subunits that formed at different times and/or locations. Comets probably have physical structure on comparable scales. Whipple's (1950) characterization of a comet as a ''dirty snowball'' had the unintentional connotation (at least for those with experience of terrestrial snowballs) of a monolithic body with substantial strength; however, comets display mechanical weakness by shedding fragments or splitting into pieces. Such events have inspired models of cometary nuclei as ''rubble piles'' (Weissman 1986), aggregate bodies resembling bunches of grapes (Jewitt and Meech 1988), or fractal structures (Donn and Hughes 1986). Theories that envisage their formation directly from microscopic grains (Biermann and Michel 1978, Hills 1982, Bailey 1987) cannot account for such structure.

The structural weakness of comets was demonstrated dramatically by Shoemaker–Levy 9 (SL9), which disrupted during a close encounter with Jupiter. If this disruption was due to the jovian tidal forces (rather than collision with a ring particle), the parent comet must have been weaker than a monolithic body composed of any plausible geological material. The simulations of tidal disruption by Asphaug and Benz (1996) imply an internal strength of no more than $\sim 10^{-3}$ bar, and are consistent with zero strength, i.e., only gravitational binding of a ''rubble pile'' structure. Such low strength is also consistent with the behavior of other comets. The best match of the Asphaug and Benz results to observations suggests that the comet had a diameter $\simeq$2 km and density $\simeq$0.5 g cm^{-3}, and disrupted into at least a few hundred components that reaccreted into the $\simeq$20 visible subnuclei. These results imply that the components had sizes $\lesssim$100 m, and could have been much smaller.

I tentatively accept the properties of SL9 as typical for a small comet. Much larger comets are known; Chiron has a diameter 180 km, and objects in the Kuiper disk may be as large as 300 km. Thus, whatever process(es) formed comets in the outer solar nebula produced bodies with a range of sizes from ~1 km to 100 km. At least the smaller ones consist of low-density, weakly bound assemblages of still smaller components. The larger Chiron-sized bodies are presumably compacted to some degree by gravitational self-compression.

The purpose of the present paper is to present a self-consistent model of the formation of comets as icy planetesimals. I show that beginning with microscopic grains in the solar nebula, their accretion into macroscopic objects can produce bodies having the observed properties of cometary nuclei, in particular, low strength and structural components on scales ~100 m. These properties are a natural outcome of the accretion process within the gaseous nebular disk.

II. PARTICLE MOTIONS IN THE SOLAR NEBULA

Small solid bodies in the solar nebula were strongly influenced by the presence of the nebular gas. Drag forces were important during the formation of planetesimals. This is in some sense a matter of definition, as in this paper I define a ''planetesimal'' as a solid object large enough so that the Sun's gravitational force is more important than drag in determining its dynamical behavior. The formation of planetesimals in the inner Solar System has been the subject of intensive analytical and numerical modeling (Safronov 1969, Goldreich and Ward 1973, Weidenschilling 1980, 1988, Nakagawa *et al.* 1981, 1986, Weidenschilling and Cuzzi 1993). The process in the outer part of the solar nebula was qualitatively similar, but with differences due to the larger heliocentric distances: lower temperature and surface density, larger fraction of solids due to the presence of ices, etc. One important difference of the present work from these earlier references is a reassessment of the role of gravitational instability in the process of planetesimal formation, as will be seen below.

The nebular gas is supported by pressure forces. A vertical (out-of-plane) pressure gradient allows the nebular disk in hydrostatic equilibrium to have a finite thickness or scale height. There is inevitably a radial gradient as well, due to the radial variation of surface density and temperature, as well as the general decrease in the Sun's gravitational pull with distance. This radial pressure gradient supports the gas against the Sun's gravity, causing it to rotate at slightly less than the local Kepler velocity at any given distance (Whipple 1972). The fractional deviation of the gas from Keplerian rotation is comparable to the ratio of its thermal energy to its orbital kinetic energy (Weidenschilling and Cuzzi 1993). This is typically a few parts in 10^3, giving a difference between the Kepler velocity V_K and gas velocity V_g, $\Delta V = (V_K - V_g)$, of a few tens of meters per second.

A solid particle is much denser than the gas, and so is not supported by either the vertical or radial pressure gradient. It tends to settle toward the central plane of the nebular disk and similarly drifts radially inward. The rate

at which the particle moves is determined by the drag exerted on it by the gas. In the solar nebula the appropriate drag law is generally either the Epstein or Stokes law, depending on whether the particle is smaller or larger than the mean free path of the gas molecules (Weidenschilling 1977). A critical parameter for the particle's dynamical behavior is its response time, $t_e = mV/F_D$, where m is the particle's mass, V its velocity relative to the gas, and F_D the drag force (which may depend on V). The Kepler time scale is the inverse of the orbital frequency Ω, defined as $\Omega = (GM_\odot/R^3)^{1/2}$, where R is the distance from the Sun, G the gravitational constant, and $M_\odot$ the solar mass. This is the time scale on which the Sun's gravity affects the particle's motion. The ratio of the drag response time to the Kepler time determines the dynamical regime. If $t_e\Omega \ll 1$, the particle is strongly coupled to the gas, and drag forces constrain it to move with the gas (the gas itself is in nearly Keplerian motion due to the Sun's gravity). When $t_e\Omega \gg 1$, gravity dominates and the particle pursues a Keplerian orbit, with drag a minor perturbation on its orbital motion on time scales longer than its orbital period. As t_e is dependent primarily on the mass/area ratio, which increases with size, small particles are strongly coupled to the gas, and large ones weakly coupled. In the discussion that follows, I define "small" particles as those with $t_e\Omega < 1$ and "large" as $t_e\Omega > 1$. For typical low-mass ($\lesssim 0.1M_\odot$) nebular models, the transition between "small" and "large" is at sizes of the order of 1 m. The transition size is insensitive to heliocentric distance, because the decrease in gas density at larger distances increases t_e as Ω decreases (Weidenschilling 1977).

The motion of a particle in the nebular gas has been described in detail by Adachi *et al.* (1976) and Weidenschilling (1977). To summarize briefly, small particles move with the angular velocity of the gas, but drift radially toward the Sun at velocities that increase with particle size (or t_e). Large particles travel in Keplerian orbits, and feel a "headwind" of magnitude ΔV from the slower-moving gas. Their orbits decay at a rate that decreases with size (or t_e). The radial velocity reaches a peak equal to ΔV at the transition size where $t_e\Omega = 1$. This behavior is seen in Fig. 1, which shows the velocity components of a particle relative to the gas at a heliocentric distance of 30 AU. The nebular parameters chosen yield $\Delta V = 54$ m sec^{-1}.

The noteworthy feature of Fig. 1 is the size dependence of particle velocities. For small particles ($d \lesssim 100$ cm), the radial drift velocity is much greater than transverse velocity relative to the gas. Large bodies have high transverse velocity, of magnitude ΔV, relative to the gas; however, this transverse velocity is independent of size. Radial velocities of the large bodies are size dependent, and exceed the escape velocity for sizes less than about 1 km. Thus, relative velocities between pairs of bodies of different sizes but in the same regime (both small or both large) are dominated

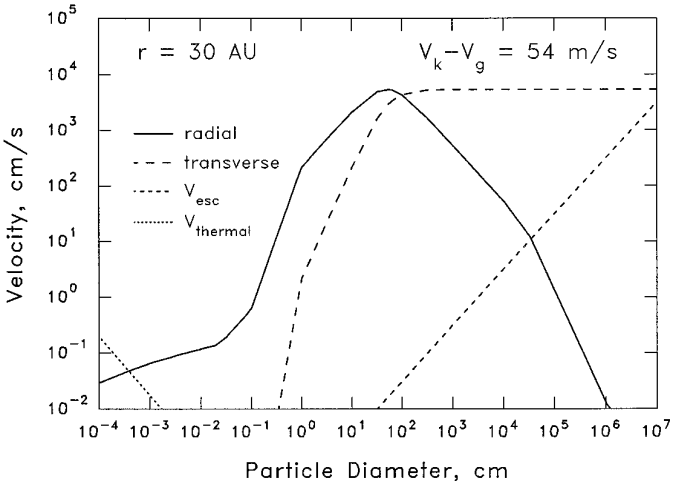

FIG. 1. Particle velocities as functions of size in the model nebula at 30 AU. Particles are assumed to have a fractal structure at sizes 10^{-2} cm, and constant density 0.7 g cm^{-3} at $d > 1$ cm. Dotted line: thermal velocity at $T = 50$°K. Solid line: radial velocity, with peak value equal to $\Delta V = 54$ m sec^{-1} at $d \simeq 10^2$ cm. Changes in slope are due to variation of particle density ($d \leq 1$ cm) and transition from Epstein to Stokes drag law ($d \sim 10^5$ cm). Dashed line: transverse velocity relative to pressure-supported gas. Short dashes: escape velocity from the particle's surface.

by their radial motions. Here we neglect turbulence which can cause an additional component of relative velocity with different size dependence; however, its contribution to relative velocities is likely to be unimportant compared with the drift velocities. For small particles, velocities induced by turbulent eddies are correlated, while large particles are decoupled from the eddies (Weidenschilling 1984). Thus, relative velocities are less than the velocity of the turbulence. It is customary to define the viscosity of a turbulent accretion disk as $\nu = \alpha cH$, where c is the sound speed and $H \sim c/\Omega$ is the scale height, with α a dimensionless coefficient. Viscosity can also be expressed as the product of the turbulent eddy velocity V_t and a mixing length; the latter is of the order V_t times the eddy turnover time, $\sim\Omega^{-1}$. This gives $\nu \sim V_t^2/\Omega$, or $\alpha \sim (V_t/c)^2$. In our example, turbulent velocity of magnitude ΔV (extending throughout the thickness of the nebula) would correspond to a viscosity parameter of $\alpha \sim 10^{-2}$. For smaller values of α, relative velocities are dominated by differential drift.

III. FORMATION OF PLANETESIMALS/COMETESIMALS

A general picture of the early stage of planetesimal formation has been developed by analytical and numerical studies (Safronov 1969, Goldreich and Ward 1973, Weidenschilling 1980, 1988, Nakagawa *et al.* 1986, Weidenschilling and Cuzzi 1993). From a somewhat artificial assumed initial stage of micron-sized grains suspended

uniformly in gas, growth begins with thermal brownian coagulation. Grain aggregates begin to settle toward the central plane of the nebula. As larger aggregates settle faster, they sweep up smaller ones and ''rain out'' in a form of ''runaway growth.'' The aggregates grow to sizes of order centimeters, and form a dense layer in the central plane. As settling velocities greatly exceed the escape velocities of particles of this size, the growth process at this stage depends on surface forces and mechanical interlocking of aggregates rather than gravity (cf. Dominik and Tielens 1997).

Different processes have been suggested to produce large planetesimals from this layer of centimeter-scale aggregates. Safronov (1969) and Goldreich and Ward (1973) maintained that if the layer reached a density greater than a critical value, it would become unstable and collapse under its own gravity into kilometer-scale bodies; however, this gravitational instability requires the space density of particles to be much greater than that of the gas. In that case, the particles, rather than gas, dominate the dynamics of the layer. Lacking pressure support, the particle layer must attain nearly Keplerian rotation, resulting in shear between it and the surrounding gas. Weidenschilling (1980) showed that this shear flow was unstable and would cause the layer to become turbulent; the turbulence would prevent the particle layer from attaining the critical density for gravitational instability. These conclusions were confirmed by detailed numerical modeling by Cuzzi *et al.* (1993). Thus, a layer of small particles that was well coupled to the gas could not become gravitationally unstable. The formation of planetesimals required collisional coagulation, at least to sizes large enough to decouple from the shear-induced turbulence, i.e., at least meter-sized.

This conclusion left open the possibility that kilometer-sized or larger planetesimals formed by gravitational instability, only in a layer of meter-sized, rather than centimeter-sized, bodies; however, two other factors prevent gravitational instability from being effective. Attaining a critical density is a necessary, but not sufficient, condition for instability. The velocity dispersion of the particles must also be less than a critical value (Weidenschilling 1994). The radial velocity dispersion due to drag decreases as the mean particle size increases; this implies that coagulation must produce bodies tens of meters in size before the conditions for instability are met. After this occurs, there is yet another obstacle to the formation of planetesimals by gravitational instability. Bodies as large as tens of meters retain a velocity dispersion that is not damped significantly by collisions or drag. The lack of damping prevents instabilities on scales small enough to form solid planetesimals. If instability occurs, it is only on large scales that produce gravitationally bound clusters of bodies; these are stabilized by rotation and cannot collapse (Weidenschilling 1995).

This line of reasoning leads to the conclusion that comets and any other planetesimals that formed in the solar nebula did so by collisional coagulation. Their growth required some non-gravitational sticking mechanism(s) that allowed net gain of mass in collisions. For grains and small aggregates, van der Waals surface forces, and perhaps electrostatic forces, were adequate. Growth of macroscopic bodies probably involved mechanical interlocking of irregular surfaces. The size dependence of drag-induced velocities is an aid to coagulation: bodies of comparable size would have low relative velocities, and hence were unlikely to fragment or disrupt in collisions. Most drag-driven impacts would be between bodies of very different sizes. While impact velocities could be high (as large as ΔV, tens of m $\sec^{-1}$), the smaller body would not have enough kinetic energy to disrupt the larger. If the large body were a loose aggregate, the projectile would simply bury itself in the target, with the possibility of net mass gain. The outcome obviously depends on the mechanical properties of the bodies, which are not known; however, plausible assumptions do allow growth in collisions, as will be shown below.

In summary, comets and other planetesimals formed by collisional coagulation rather than gravitational instability. Large-scale instabilities may have affected the local space density of solid bodies and, hence, the time scale for their growth, but had no other effect. Collisions were caused primarily by differential radial velocities, induced by gas drag acting on bodies of different sizes. This method of growth and the dependence of velocity on size has interesting consequences for the structure of the growing planetesimals, as seen in the results of numerical modeling.

IV. NUMERICAL MODELING OF COMETARY FORMATION

The numerical model has been described earlier (Weidenschilling 1980, 1984, 1988, Weidenschilling and Cuzzi 1993). The present simulation is carried out to a much later stage than these earlier efforts, which were stopped when the particle layer reached the ''classical'' critical density. With the understanding that this condition is not sufficient for gravitational instability, and that instability does not cause collapse to planetesimals, it is possible to continue simulations past this point. We can now model the growth of particles from micrometer to kilometer sizes, through the transition between the drag-dominated and gravity-dominated regimes. I provide a general summary of the model here, with details of the algorithms in Appendixes A–G. The model is one-dimensional, computing the local size distribution of particles at various distances from the central plane of the nebula at a given heliocentric distance. The evolutionary timescale and radial drift rates imply that particles can undergo significant radial migration, so a two-dimensional model is needed for a rigorous

solution. This has been impractical thus far because of the computational demands of such a model. I note that the vertical gradient of the particle distribution is much steeper than the radial gradient, so the present model is more realistic than one that has radial resolution, but employs vertical averaging through the nebular disk (Mizuno *et al.* 1988).

The particle size distribution is computed in a series of levels at different distances from the central plane. Relative velocities are computed due to thermal motion, turbulence (where present), vertical settling, and systematic motions induced by the gas; the latter are usually dominant. The particle concentrations and velocities yield collision rates between bodies of all sizes. Collisional outcomes depend on the assumed mechanical properties (impact strength), impact velocities, and sizes of projectile and target. Possible outcomes include sticking, cratering with net gain or loss of mass by the target, and disruption (Appendix F).

Particles are transferred from one level to another during each time step. Systematic settling operates in only one direction, toward the central plane. For particles that are small (in the dynamical sense, $t_e\Omega < 1$), the vertical settling velocity is used in a straightforward manner. For large particles, the ''settling'' rate used is actually the rate at which drag damps the inclination of a Keplerian orbit. When turbulence is present, it can transfer particles both upward and downward. The present model and the author's earlier work include this turbulent flux in both directions [contrary to the statement by Dubrulle *et al.* (1995) that the model lacked this feature]. For small particles, their flux is treated as simple diffusion, using a standard formulation of turbulent diffusivity. Large bodies are in orbits perturbed by randomly directed turbulent velocity impulses. Treating this case as classical diffusion can yield nonphysical results; I use a modified diffusion approximation for large bodies (Appendix D).

At the start of a simulation all of the solid material is in the form of grains of diameter 10^{-4} cm. The solids/gas mass ratio is uniform at all levels, and is set to 0.015, consistent with condensation of H_2O ice. Initially there are 12 levels ranging from $z = 0$ (in the central plane) up to twice the scale height of the gas. Whenever settling and coagulation produce a significant difference in the particle concentration or size distribution between the two lowest levels, the lowest one is divided into two levels. This procedure yields progressively higher spatial resolution near the central plane as the particle layer forms and evolves. The maximum number of levels, 23, gives a resolution 3×10^{-6} times the gas scale height, which is necessary to model the vertical distribution of particles in the thin, dense layer.

When the density of the particle layer exceeds that of the gas, coupling between particles and gas reduces ΔV from the pressure-supported value far from the central plane. The particle–gas layer rotates more rapidly, at a velocity determined by the particle mass loading and size distribution. Nakagawa *et al.* (1986) derived this velocity for the case of a single effective particle size; I generalize it to the case of a distribution of sizes (Appendix B). This shear is assumed to generate turbulence with eddy velocities proportional to the difference between the local gas velocity and the pressure-supported value. The intensity of turbulence therefore varies at different levels within the particle layer. The turbulence is characterized by a Rossby number, Ro, the ratio of eddy frequency to the Kepler frequency (Cuzzi *et al.* 1993), and is assumed to have a Kolmogorov spectrum, as described in Appendix D.

Turbulence has the greatest effect on small particles that are strongly coupled to the gas and a lesser effect on larger ones. For the largest bodies, mutual gravitational stirring must eventually dominate relative velocities. I parameterize gravitational stirring of large bodies by a Safronov number θ, which scales velocities to the escape velocity of the median-mass bodies in the particle layer (Appendix E), with additional assumptions of equipartition of kinetic energy among bodies larger than the median mass. Relative velocities between particles are the difference in systematic radial, transverse, and vertical velocities induced by drag, summed quadratically with the random velocities due to turbulence and gravitational stirring. In this manner the simulation can span the entire range of particle sizes from micrometers to kilometers. The presence of shear-generated turbulence and the need to resolve the structure of the thin particle layer impose a strong limit on the allowed time step. Its size must be less than $\Delta z/V_t$, where Δz is the thinnest zone and V_t the turbulent velocity. A complete simulation requires $>10^6$ time steps to grow kilometer-sized bodies from micrometer-sized grains.

V. RESULTS

The nominal case for cometary formation assumes a low-mass solar nebula at heliocentric distance 30 AU. The surface densities of gas and solids are 29 and 0.41 g cm^{-2}, respectively. The assumed temperature of 50 K gives a gas density of 3×10^{-13} g cm^{-3} at $z = 0$ and a scale height, H, of 3.3 AU. The deviation of the gas from Keplerian motion is $\Delta V = 5.4 \times 10^3$ cm sec^{-1}. The grains are initially distributed with the same scale height as the gas (uniform solids/gas ratio), and have diameter 10^{-4} cm. Single grains have density 1.0 g cm^{-3}; aggregates are assumed to have fractal structure of dimension 2.1 at sizes 10^{-4} to 10^{-2} cm and uniform density 0.7 g cm^{-3} at sizes larger than 1 cm. Their impact strength is taken to be 10^6 erg g^{-1}.

The evolution is qualitatively similar to earlier simulations done for smaller heliocentric distances (Weidenschilling 1980, Weidenschilling and Cuzzi 1993). There is an initial period of slow thermal coagulation with no significant settling, which lasts for a few times 10^4 years. Eventu-

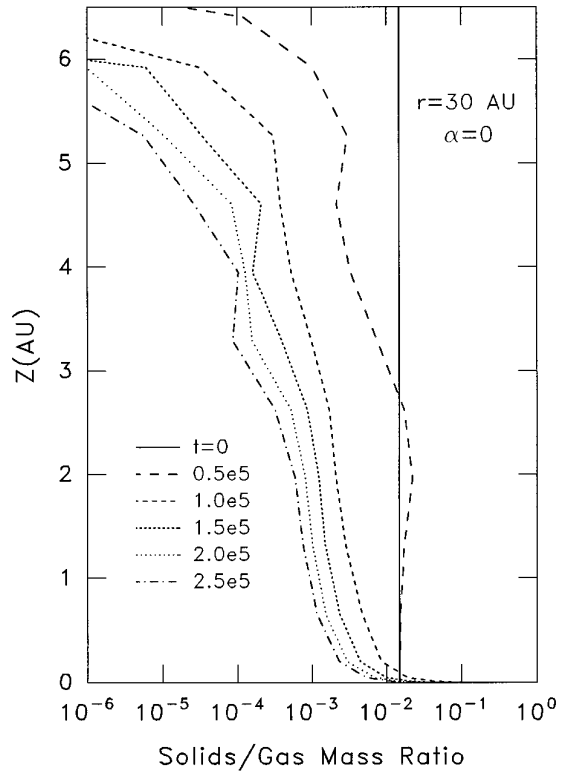

FIG. 2. Solids/gas mass ratio versus distance from central plane (z) at different times. Initial value assumed to be 0.015 at $t = 0$. Here and in the following figures the notation $\alpha = 0$ indicates that there is no turbulence other than that generated locally by shear in the particle layer.

ally the largest aggregates reach sizes such that their settling velocities exceed their thermal motion, and "rainout" begins. The concentration of solids in the central plane rises abruptly at $t \simeq 5 \times 10^4$ years, in the form of aggregates a few centimeters in size. The higher space density of solid particles, which are still well coupled to the gas, initiates shear flow and turbulence. The half-thickness of the turbulent region is initially $\simeq 0.025H$ (0.08 AU); however, the turbulent velocity is not sufficient to prevent settling as the particles continue to grow. The region with enough mass loading to drive shear and turbulence decreases in thickness to $<2 \times 10^{-3}H(\simeq 6 \times 10^{-3}$ AU) after $\simeq 10^5$ years.

Figure 2 shows the evolution of the vertical distribution of solids over the full range of the calculation, from $z = 0$ to $2H$. On this scale, the dense, turbulent layer in the central plane is unresolved. Though the rest of the thickness of the nebula, the concentration of solids decreases due to settling. The vertical distribution of solids in the turbulent region near the central plane is shown in Fig. 3. Note that this region is extremely thin; the vertical scale is expanded by a factor of 10^3 from Fig. 2, and the region shown is essentially the entire half-thickness of the turbulent layer. The concentration of solids varies substantially within this layer on a much smaller scale ($<10^{-4}$ AU); it will be shown that this fine structure is due to the size distribution of particles, where the larger ones are less affected by turbulence and settle into a thinner sublayer. The solids/gas mass ratio reaches a peak value $>10^3$ in the sublayer at $t \simeq 10^5$ years. Continued growth allows gravitational stirring to become effective for the largest bodies after this time; the sublayer then thickens while its density decreases.

The particle layer drags the entrained gas with it at higher speed than the pressure-supported value, reducing the effective value of ΔV. This is taken into account when solving for the drag-induced velocities at each level within the particle layer. The lower ΔV lowers the peak values for radial and transverse velocities, but the general shapes of the plots in Fig. 1 are preserved, and the size at which the peak velocities are reached is unchanged. The variation of ΔV with time at $z = 0$ is shown in Fig. 4. The sharp drop at $t = 6 \times 10^4$ years is due to the rapid increase of mass loading due to "rainout" of centimeter-sized aggregates, which are well coupled to the gas. The mass loading in the central plane continues to increase with time, but growth of the particles decreases their coupling to the gas. The effective ΔV gradually approaches the free-stream value

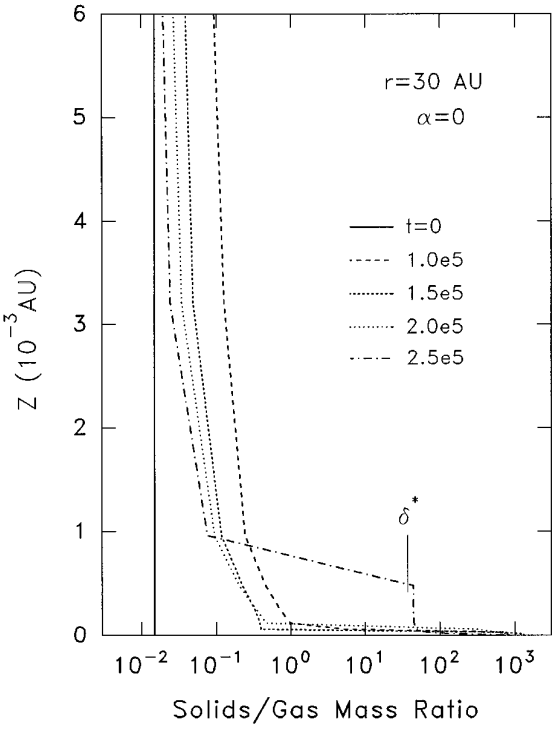

FIG. 3. Solids/gas mass ratio near the central plane. Vertical scale is expanded by a factor of 1000 from Fig. 2. δ^* is the critical density for "classical" gravitational instability. The peak value of the solids/gas ratio exceeds 10^3 in the very thin sublayer of large particles. At 2.5×10^5 years, the sublayer "puffs up" due to gravitational stirring by the largest bodies.

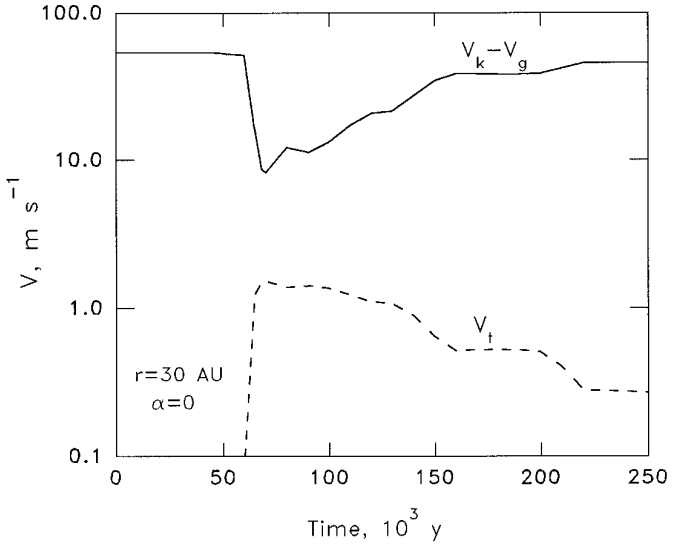

FIG. 4. Deviation of the gas velocity from the Kepler velocity in the central plane of the nebula. At $t = 0$, ΔV has the "free-stream" value of 54 m sec^{-1}. Formation of the dense particle layer drags the gas with it, decreasing ΔV to $\simeq$10 m sec^{-1}. As their mean size increases with time, the particles decouple from the gas, allowing ΔV to increase. Dashed line: turbulent velocity induced by shear between the particle layer and surrounding gas.

as the mean particle size increases. Note that the effective ΔV has a minimum at about 20% of the free-stream value; the particle layer never attains Keplerian rotation. Also shown in Fig. 4 is the turbulent eddy velocity induced by the shear flow. Its peak value is about 150 cm sec^{-1}. At all times the systematic drift velocities induced by drag are greater than the random velocities due to turbulence.

The optical thickness of the nebula follows a similar pattern. Figure 5 shows the integrated optical thickness (based on Rosseland mean opacity) due to solid grains, above any given level. Details of the opacity calculation are given in Appendix G. The initial optical half-thickness of the nebula is $\simeq$7 at $t = 0$, and decreases by about an order of magnitude during 2×10^5 years of evolution. The high concentration of solids in the central plane makes no contribution to the opacity because its mass is concentrated in large bodies.

The particle layer's density in the central plane reaches the critical value for "classical" gravitational instability (Goldreich and Ward 1973) at $t = 6.84 \times 10^4$ years. At this time the median particle mass corresponds to diameter 1.3 m, with the largest bodies having $d = 6.7$ m. Gravitational instability does not occur at this point, however, due to the large radial velocity dispersion of the particles. The criterion that the mean radial velocity must be less than a critical value (Weidenschilling 1994) is met at 8.94×10^4 years, when the median-mass bodies have $d = 27$ m and the largest bodies have $d \simeq 100$ m. At the time instability occurs, the actual space density of particles in the central plane is $\simeq$16 times the "classical" threshold. Bodies of size tens of meters are poorly damped by collisions or drag. As argued by Weidenschilling (1995), the velocity dispersion prevents gravitational instability on small scales. Instability occurs only on a large scale, which is most susceptible to density perturbations. The length scale of this instability is $\lambda^* \sim 2\pi^2 G\sigma\Omega^{-2}$, where σ is the surface density of the particle layer (not the total surface density of solids in the nebula). In the present simulation, counting all levels for which the local space density exceeds the classical threshold, about two-thirds of the total solids take part in the instability. The appropriate parameters yield $\lambda^* \simeq$ 0.016 AU, and the condensations have masses of order $\sigma\lambda^{*2} \sim 1.6 \times 10^{22}$ g. If combined into a single body of density 1.0 g cm^{-3}, this mass would correspond to a diameter $\simeq$300 km; however, condensations of this size have too much angular momentum (from the approximately Keplerian rotation of the particle layer) to collapse to solid bodies. The large-scale gravitational instability merely produces gravitationally bound clusters of bodies which continue to grow within those clusters by collisions. The net effect of instability may simply be an increase in the local

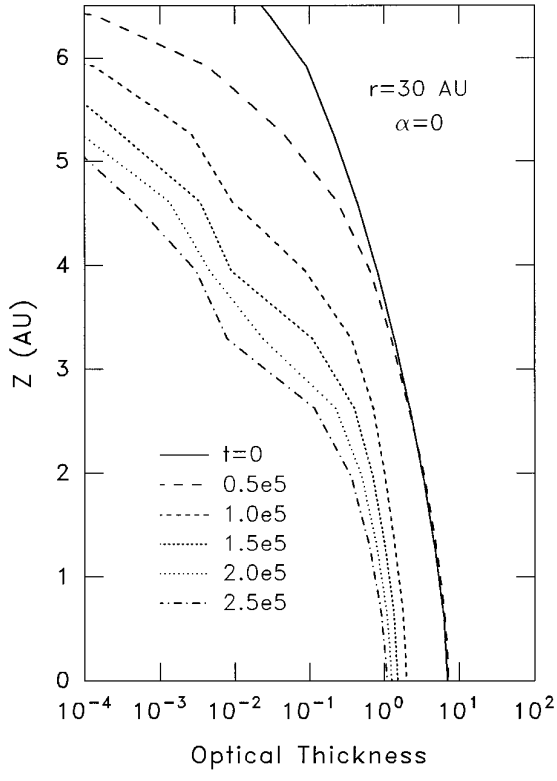

FIG. 5. Integrated optical thickness above height z, computed using Rosseland mean opacity for the mass loading and size distribution of particles at each level. Vertical distribution changes because of settling; total optical thickness decreases due to particle growth.

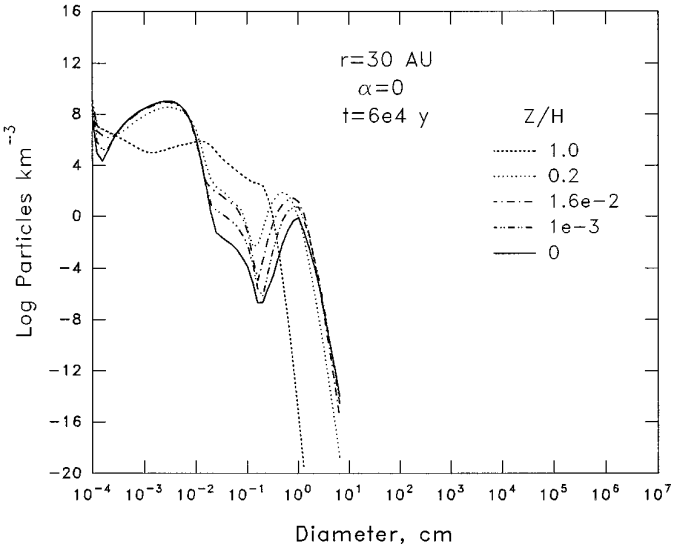

FIG. 6. Particle size distribution at different elevations, z, in units of gas scale height, H; units are particles km^{-3} per logarithmic diameter interval of $2^{1/3}$. Here and in following figures, the solid line is for the central plane ($z = 0$), which contains most of the mass; the vertical resolution varies with the thickness of the particle layer. At 6×10^4 years, the bimodal size distribution is due to thermal coagulation and vertical settling, which dominate at different sizes.

space density of particles within a cluster, shortening the time scale for accretion. In the present simulation I ignore this effect, and simply continue the calculation after the onset of gravitational instability. In Section VII, I consider some possible consequences of gravitational clustering.

VI. SIZE DISTRIBUTION OF COMETARY COMPONENTS

The preceding results are not subject to any observational verification, but the size distribution of the comets and any substructure within their nuclei are observables of great interest. Future space missions to rendezvous with comets may constrain the process of their formation. Figures 6–12 show the computed evolution of the particle size distribution during accretion. The data are presented as numbers of bodies per volume per logarithmic interval of diameter (each size bin spans a width of $2^{1/3}$). In each figure the solid line shows the size distribution in the central plane, where most of the mass is concentrated. The other lines (dashed) give size distributions at other levels, with z in units of the gas scale height H.

At 6×10^4 years (Fig. 6), the particle mass density exceeds that of the gas, and shear has begun to produce turbulence in the central plane. The size distribution at small values of z is bimodal, with one peak at a few times 10^{-3} cm due to thermal coagulation. Most of the mass is in the other peak, which consists of approximately centimeter-sized aggregates formed during the "rainout" from higher levels; these grew by sweeping up grains and smaller aggregates while settling vertically.

By 7×10^4 years (Fig. 7), most of the growth at $z = 0$ is due to radial drift, with larger aggregates sweeping up smaller ones. The size distribution is no longer bimodal, but resembles a power law. This is the result of erosion during collisions among the larger bodies, which replenishes the supply of smaller particles at all sizes. Despite this erosion, the larger bodies still have a net mass gain and continue to grow.

At 8×10^4 years, the size distribution has developed a distinct peak at $d \sim 20$ m, separated from the smaller-size population by a valley at sizes approximately a few meters (Fig. 8). As time progresses, the peak and valley become more prominent, leaving a virtually depopulated gap at $d \sim 5$ m. Essentially all of the mass is in the peak at large sizes, centered on $d \simeq 100$ m by 1.5×10^5 years (Figs. 9 and 10). Finally, the peak begins to broaden at $\sim 2 \times 10^5$ years, as bodies larger than kilometer size become more abundant (Fig. 11), and gravity-dominated runaway growth begins (Fig. 12).

The reason for the development of the peak in the size distribution is found in Fig. 1, the plot of particle velocity versus size. Recall that at sizes less than about 1 km, drag-induced velocities are more important than gravitational stirring, and the dominant component of relative velocity between bodies of different sizes is radial motion. The radial velocity has its peak at $d \sim 1$ m (the actual size at the peak depends on the densities of both the particle and the gas, but is insensitive to heliocentric distance; cf.

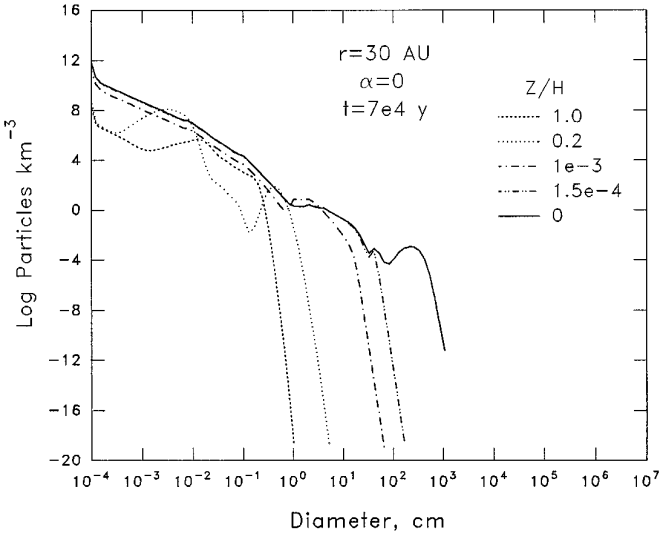

FIG. 7. Size distribution at 7×10^4 years. For $z = 0$ it resembles a power law due to erosion of the larger (meter-sized) bodies, which replenishes the population of small particles.

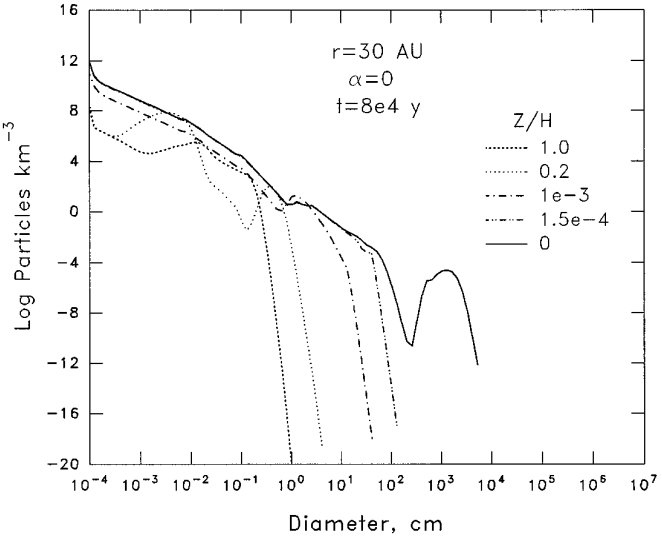

FIG. 8. At 8×10^4 years, a peak is developing at $d \simeq 10$ m, while m-sized bodies are being depleted by collisions with the larger objects.

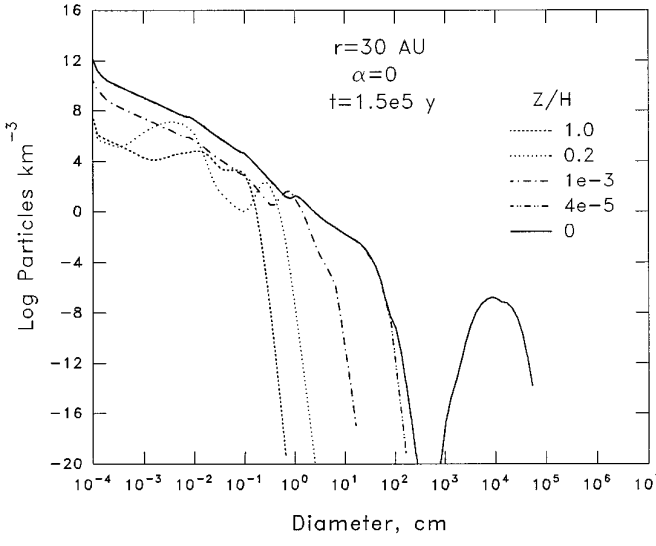

FIG. 10. At 1.5×10^5 years, the mass peak is at $\simeq$100 m, while the largest bodies are still smaller than kilometer-sized.

Weidenschilling 1977). Radial velocities decrease at larger sizes.

During the early stage of growth to meter-sized bodies the size distribution is broadened because the larger bodies have higher velocities and collision rates than the smaller ones and, thus, grow faster. After accretion has produced a population of bodies larger than the size corresponding to the peak velocity, the approximately meter-sized bodies that exist then, or form after that time, are rapidly depleted; because of their high radial velocities, they soon collide with a larger body. This depletion is the cause of the "valley" in the size distribution in the diameter range ~1–10 m.

The larger bodies, tens to hundreds of meters in size, have velocities that decrease with size. As they grow, their relative velocities and the rate of collisions decrease. Their radial velocities, and the concomitant velocity dispersion, are still much greater than their escape velocities, so there is no enhancement of their collisional cross sections by

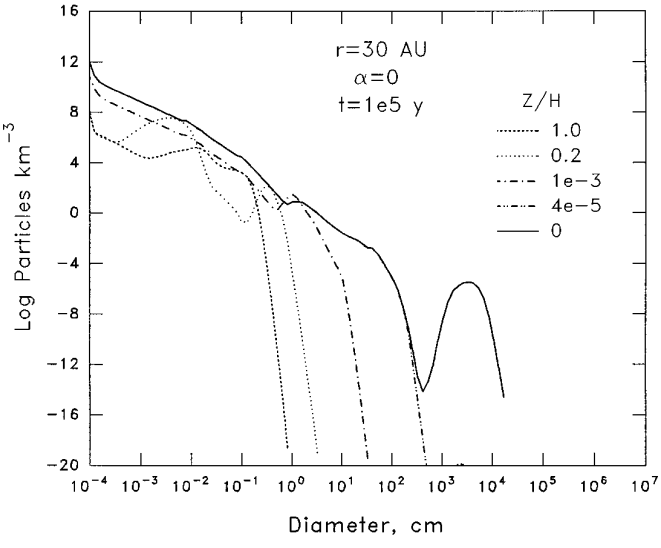

FIG. 9. At 10^5 years, most of the mass is in bodies of size ~10–100 m, with the mass peak at $\simeq$30 m.

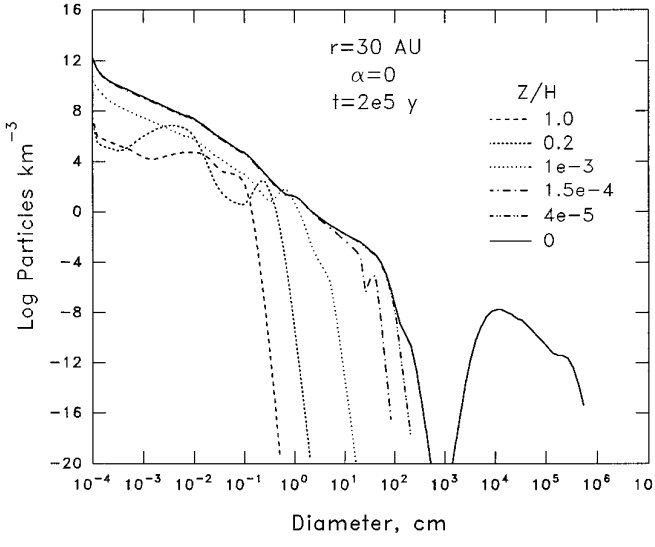

FIG. 11. At 2×10^5 years, bodies larger than $\simeq$1 km begin to have higher growth rates due to gravitational focusing, which increases their collisional cross sections. Gravitational stirring becomes more important than gas drag for determining relative velocities. The size distribution broadens again.

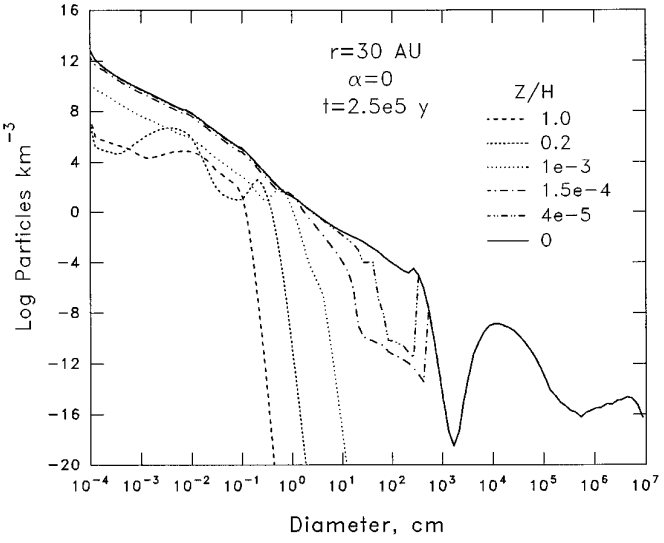

FIG. 12. At 2.5×10^5 years, most of the mass is in bodies >10 km in size produced by gravitational accretion. The peak at $d \sim 100$ m consists of "leftover" bodies from drag-driven accretion. Fragments produced during collisions of the larger bodies have begun to fill in the "valley" at $d \sim 10$ m, and supply the power-law "tail" of small particles.

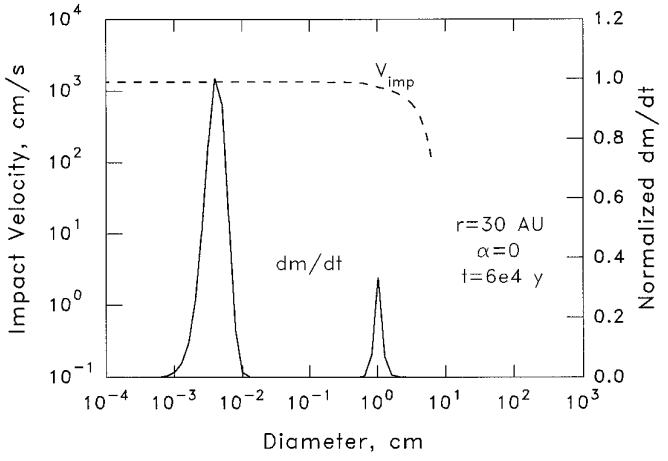

FIG. 13. Solid line: the rate at which mass is added to the largest body in the size distribution from the various size bins containing smaller particles, normalized to the peak value. Dashed line: impact velocities of smaller bodies colliding with the largest body. At 6×10^4 years, the largest bodies are ≃10 cm in size, and gain most of their mass from aggregates of size ≃30–50 μm impacting at ≃10^3 cm sec^{-1}.

gravity. The slower growth of the larger bodies tends to keep the "peak" in the size distribution narrow and produces a sharp cutoff at the large end of the size distribution (an analogous situation is thermal coagulation, which also tends to produce a narrow size distribution because of lower velocities at higher masses). Growth in the range approximately meters to kilometers is the opposite of the "rainout" phase, where larger aggregates outgrow smaller ones, or the more familiar "runaway growth" in gravitational accretion, where the larger bodies grow more quickly due to their gravitational cross sections (Wetherill and Stewart 1993). The pattern of slower growth with a narrow peak in the size distribution continues until the decreasing drag-induced velocities and larger escape velocities allow gravitational cross sections to influence the collision rate. The larger bodies then regain their advantage, and the size distribution broadens, as seen in Fig. 11. After this time, accretion is dominated by gravitational forces, and the effects of gas drag become unimportant.

How do this velocity dependence and the size distribution that it produces affect the structure of the accreting cometesimals? I try to answer that question by Figs. 13–19. Each of these shows, for the largest body that has accreted at that time, the impact velocities of all smaller-sized bodies that could collide with it (dashed line); this depends on the value of ΔV at that time (Fig. 4). Also shown is the actual rate at which mass is being added by impacting bodies of various sizes, which depends on the size distribution at that time. For example, one may infer from Fig. 13 that at 6×10^4 years, the largest bodies had $d \simeq 10$ cm (the right-hand end of the dashed line). A body of this size was growing by accreting grain aggregates 30–50 μm in diameter, which impacted at ~10^3 cm sec^{-1}. At 7×10^4 years (Fig. 14), the largest body ($d \simeq 10$ m) grew by collisions with bodies ≃2–3 m in size, impacting at ~200 cm sec^{-1}. At 8×10^4 years (Fig. 15), the largest bodies had $d \simeq 70$ m and grew by accreting ≃20-m bodies at ~80 cm sec^{-1}. At 10^5 years, ≃200-m bodies accreted ≃50-m bodies at ≃30 cm sec^{-1} (Fig. 16), and at 1.5×10^5 years, ≃500-m bodies would accrete ≃200-m bodies at ≃20 cm sec^{-1} (Fig. 17). At 2×10^5 years, the largest bodies are ≃6 km in diameter, and grow by accreting a broader range of sizes

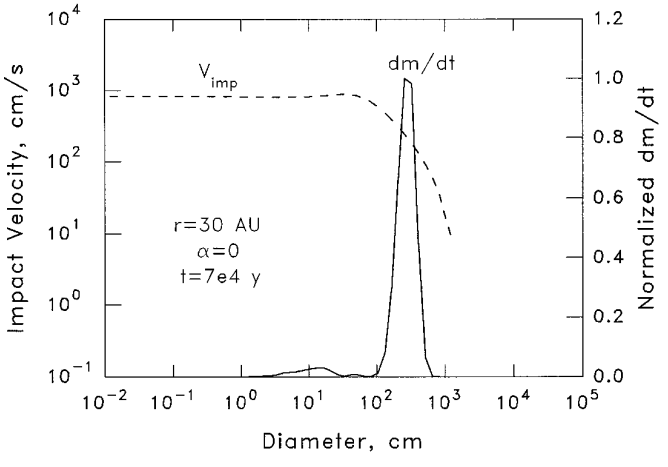

FIG. 14. At 7×10^4 years, the largest bodies have $d \simeq 10$ m and grow mainly by accreting bodies ~200–300 cm in size, impacting at ~200 cm sec^{-1}.

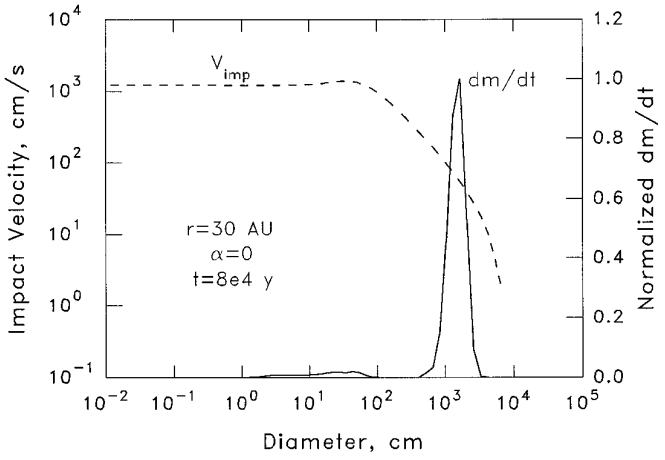

FIG. 15. At 8×10^4 years, the largest bodies are $\simeq$70 m and accrete $\simeq$20-m bodies at $\simeq$80 cm sec^{-1}.

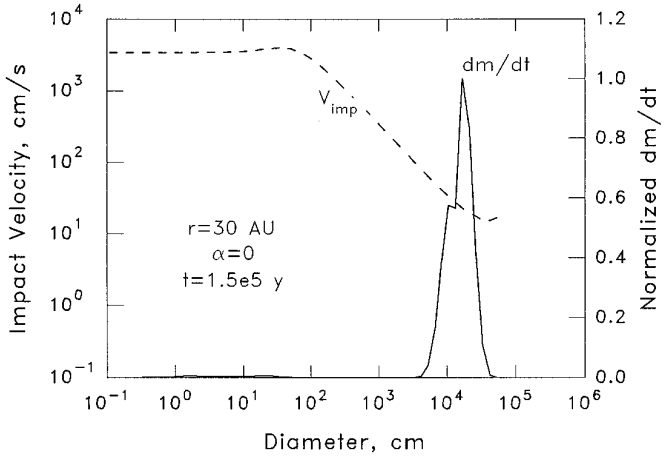

FIG. 17. At 1.5×10^5 years, the largest bodies have $d \simeq 500$ m and gain most of their mass from $\simeq$200-m bodies with impact speeds $\simeq$20 cm sec^{-1}.

with a modal value $\simeq$1 km (Fig. 18). Gravitational stirring has become significant for bodies of this size, and the escape velocity of the large target body dominates the impact velocity for projectiles larger than $\sim$10 m, although drag-induced velocities still influence the rate of impacts. The impact velocities are increasing, with values of at least $\simeq$200 cm sec^{-1}. After this point growth proceeds by gravitational accretion, in which collision rates are determined by random motions (eccentricities and inclinations) and Keplerian shear. Relative velocities and impact velocities are essentially proportional to escape velocities (Fig. 19).

Through the period of drag-controlled growth, the largest bodies typically accrete objects having masses a few percent of their own. In that respect, their growth is roughly self-similar, and might tend to produce a fractal-like structure; however, the typical impact velocities at which these bodies accrete vary significantly with size, decreasing from $\simeq$1000 to $\simeq$20 cm sec^{-1} as they grow from approximately meter to kilometer size. In this range, as bodies become larger, they are assembled more gently, due to the size dependence of gas drag. In the case of a head-on collision of two elastic spheres, it can be shown that the peak stress at the point of contact is independent of the size of the colliding bodies, and varies as the 2/5 power of the impact velocity (Timoshenko and Goodier 1951). The decreasing relative velocities as bodies grow from meter to kilometer size would correspond to a decrease in stress level by about an order of magnitude. Thus, we would expect a greater degree of compaction at the smaller size scale. What struc-

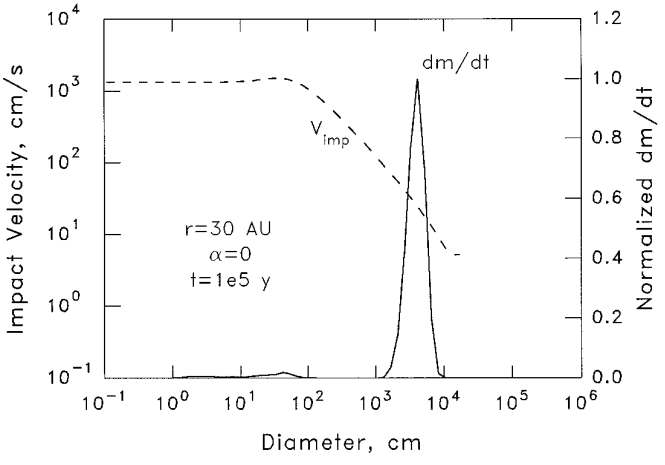

FIG. 16. At 10^5 years, 200-m bodies grow by accreting $\simeq$40-m bodies impacting at $\simeq$30 cm sec^{-1}.

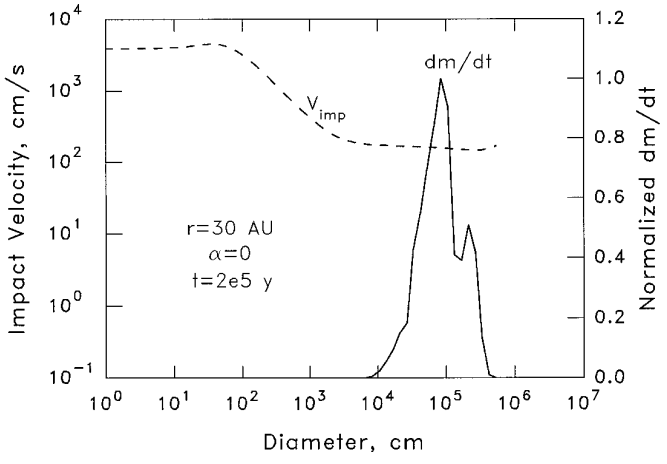

FIG. 18. By 2×10^5 years, the largest bodies have $d \simeq 6$ km. Most of their growth is by accreting kilometer-sized bodies. Impact speeds have increased to $\simeq$200 cm sec^{-1}; most of this velocity is due to the gravity of the largest bodies ($V_e \simeq 170$ cm sec^{-1}).

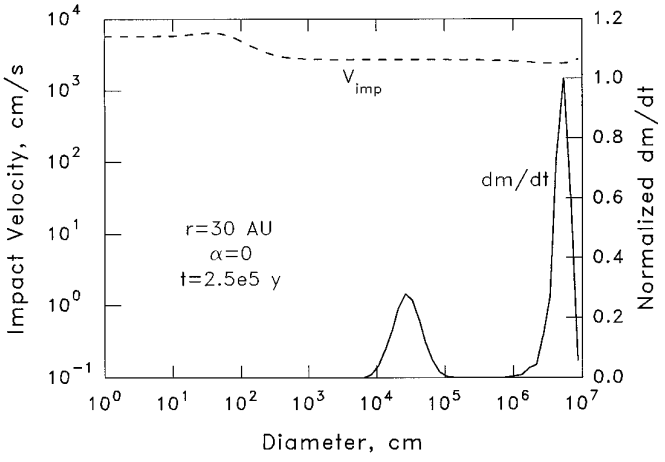

FIG. 19. At 2.5×10^5 years, the largest bodies ($d \simeq 80$ km) are growing by gravitational accretion, with impact velocities comparable to their escape velocities.

ture, if any, is preserved during accretion depends on the impact strength of the colliding bodies. Sufficiently high strength would preserve the identities of all the small components within the large aggregates, while producing a fractal distribution of void spaces. Low strength would crush the components and produce a uniform large-scale structure. As impact stresses are not evenly distributed, but are greatest near the point of contact, we can expect a variety of structures between these extremes; however, because the impact velocities have a minimum for impactors with diameters ~100 m, structure of this scale is most likely to be preserved. It is, interestingly, comparable to the scale of cometary structure inferred from observations.

VII. DISCUSSION

I have modeled the formation of cometesimals/planetesimals in the solar nebula by a "first principles" approach, beginning with microscopic grains suspended in gas and allowing the system to evolve via (one hopes) all relevant physics. The present work differs from previous efforts of this type (Greenberg *et al.* 1984, Yamamoto and Kozasa 1988) due to reconsideration of the role (or lack thereof) of gravitational instability and the recognition of the importance of drag-induced velocities for collisional coagulation. Plausible choices of parameters for the solar nebula and solid particles lead to planetesimals in the outer Solar System with properties consistent with those observed for comets. The quantitative results depend to some extent on the assumed input parameters for the nebula (surface density, gas density, ΔV), and particles (bulk density, impact strength). A full simulation is too lengthy for a complete search of parameter space; a modest exploration to date implies the results are similar for different surface densities and heliocentric distances, or moderate global turbulence from sources other than shear (provided turbulent velocities are $\lesssim \Delta V$). The model works well for higher impact strengths (or perfect sticking), but would obviously fail to produce any macroscopic bodies if their strength or "stickiness" were too low. Except in that case, the time scale for producing planetesimals is a few thousand orbital periods at any heliocentric distance. This is probably a lower limit, as the presence of additional sources of turbulence (e.g., convection), besides that generated locally by shear, would inhibit the settling process. If the lifetime of the nebula was $\sim 10^6$ years, then planetesimals formed in the presence of gas, even at the distance of the Kuiper disk.

The time scale for formation of comets in this model is shorter than the probable formation time of the nebula by collapse of the presolar cloud, and planetesimals formed more rapidly at smaller heliocentric distances. Thus, the assumption of a uniform population of small grains at some well-defined starting time is not realistic. Some coagulation presumably occurred during the growth of the nebula and the concomitant redistribution of mass and angular momentum; however, the growth of large aggregates would have been prevented by collisional destruction in vigorous turbulence (Weidenschilling 1984). As the growth of macroscopic bodies is strongly aided by settling to the central plane of the disk, formation of comets and other planetesimals may have been delayed until the turbulence accompanying nebular formation had decayed to a low level.

If comets formed in the solar nebula, the following qualitative conclusions are robust:

- Comets formed by collisional coagulation rather than gravitational instability.
- Collisions were driven by differential motions due to gas drag.
- The dependence of drag-induced velocities on particle size produced a stage in which most of the mass was concentrated in a narrow range of sizes.
- The impact velocities of accreting bodies passed through a minimum at the transition from drag-driven collisions to gravitational accretion.

This model of cometary formation implies that a typical nucleus should contain a network of interconnected macroscopic voids, in addition to microscopic porosity. This network would allow gas produced by sublimation of volatiles to migrate for large distances along the path of least resistance. Such lateral migration has been suggested by Möhlmann (1996) to explain the observations that cometary activity is often restricted to a small fraction of the surface. Distinct jets may be associated with the outlets of regions of subsurface flow, while the remainder of the surface can acquire a mantle of nonvolatile material. Kührt and Keller (1994) concluded that such a mantle or crust would need

substantial cohesive strength to prevent its levitation by gas escaping through its pores; however, the channeling of gas through macroscopic cracks rather than pores would decrease this requirement for cohesion, allowing accumulation of loose dusty regolith in inactive areas.

There are additional implications that may be fruitful for future work. The time scale for accretion and the magnitude of drag-induced radial velocities implies substantial migration during accretion. A given cometary nucleus may contain components that originated at different times and heliocentric distances. This accretional history provides at least a qualitative explanation for compositional diversity within a single comet, including variations in the dust/ice ratio (Kührt and Keller 1994). The present one-dimensional model provides at best only a crude estimate of the possible compositional heterogeneity. A summation of the radial distance traveled by a body having the (time-varying) median mass during each time step yields a value at the onset of gravitational instability of about 40% of the heliocentric distance assumed for the simulation. Most of this distance is accumulated during growth through the size range 1–10 m, at which radial velocity is greatest, and before the particle layer reaches maximum density. In a more realistic two-dimensional simulation, a growing particle would encounter different nebular conditions during migration over such distance. The time scale to form a dense particle layer is less at smaller heliocentric distance, so such bodies would likely be accreted by larger, earlier-formed bodies before they could migrate very far. The range of significant compositional mixing is probably no more than a few tens of percent if the nebular was laminar. Other sources of turbulence, e.g., convection, could stir the particle layer and decrease the collision rate, allowing more migration. Although two-dimensional models are numerically challenging, they will be worth pursuing.

Gravitational instability occurs only on a large scale that yields bound clusters of particles. Their collapse to solid bodies is inhibited by their angular momentum. Individual particles within a newly formed cluster have sizes of tens of meters, with response times to gas drag $\sim 10^3$–10^4 years. One might expect gas to damp a cluster's rotation on this time scale, allowing collapse; however, the density of solid matter within such a cluster is high enough that gas within it will, to some significant extent, rotate with the cluster. Such collective motion could extend the time scale for collapse. If the angular momentum is lost through friction in a turbulent boundary layer, a rough estimate for the turbulent stress in such a boundary layer using the method of Goldreich and Ward (1973) suggests a collapse time of order 10^6 years. Clusters would not evolve in isolation, however. If they were distributed evenly in radial and transverse directions with spacing λ^*, one can show that the time between synodic encounters would typically be of the order of their orbital period. The effects of such encounters is not clear; clusters might pass through each other, merge, or disperse. Gravitational instability might be a transient phenomenon, affecting only the time scale for collisional growth. Still, it is interesting, and perhaps significant, that the mass of such clusters would suffice to make bodies with diameters of a few hundred kilometers, comparable to the inferred sizes of the Kuiper disk objects discovered by ground-based observations. Models of collisional evolution of the Kuiper disk (Farinella and Davis 1996) suggest that bodies larger than $\simeq$50 km retain a primordial size distribution. Dynamical modeling is needed to determine whether self-gravitating clusters disperse by mutual encounters or perturbations among their components or tend to accrete a substantial fraction of their mass into a single body. If the latter case holds, then the larger Kuiper disk objects would reflect the scale of instabilities and hence the local properties of the solar nebula. Additional observations of their size distribution and any variation with orbital radius are needed to test this possibility.

Collisional evolution models imply that small (kilometer-size) short-period comets derived from the Kuiper disk are not primordial survivors, but are likely to be collisional fragments of larger (tens of kilometers) parent bodies. If so, then this history would provide an alternate explanation for ''rubble pile'' structure. The two scenarios are not exclusive, however. If small comets are ''rubble piles'' and yet are collisional products, then they had to be produced from parent bodies that were shattered but partially reaccumulated. This would be easier if the parent bodies were themselves aggregate bodies rather than monolithic. Experimental data are needed for collisions of icy objects, both monolithic and aggregate in structure, at the relatively low speeds (hundreds of m sec^{-1}) in the Kuiper disk. Numerical models of such impacts including gravitational forces (Asphaug and Benz 1996, Melosh and Ryan 1997) are also needed, both to improve collisional evolution models and to interpret structure in ''rubble pile'' nuclei as primordial or secondary. Long-period comets that were stored in the Oort cloud would not be subjected to collisions, and may better preserve their original structure.

It was Whipple (1972) who first suggested that a radial pressure gradient caused the gas of the solar nebula to deviate from Keplerian motion. It is highly appropriate that this phenomenon now appears to be fundamental to the formation of comets. The ultimate test of this and any other model of cometary origin is *in situ* observation by a space probe on a rendezvous mission. We can look forward to the Rosetta mission, which may answer some questions and undoubtedly will provide new surprises.

APPENDIX A: PARTICLE VELOCITIES

Weidenschilling (1977) derived expressions for the radial and transverse velocities of a solid particle relative to pressure-supported gas.

These equations are solved numerically for the known values of the response time t_e and the local value of $\Delta V/V_k$ at each level, which may differ from the "free stream" value because of collective particle–gas coupling (Appendix B). The radial and transverse velocities assume orbital eccentricities are small, which is an excellent approximation in this case, and are valid for all values of $t_e\Omega$.

Vertical velocities are simple in the case $t_e\Omega \ll 1$, as the settling velocity is then simply the terminal velocity resulting from a balance between drag and the vertical component of solar gravity (Weidenschilling 1980). For a large body with $t_e\Omega > 1$, the situation is more complex, as the body is essentially in a Keplerian orbit with nonzero inclination. Its inclination is damped by gas drag, and decreases with time. As the "settling rate," I take the heliocentric distance a times the rate of decrease of inclination. Using the expression for inclination damping from Adachi *et al.* (1976), and neglecting eccentricity, this is

$$\frac{dz}{dt} = z\,\frac{(0.85z/a + \Delta V/V_k)}{2t_e(\Delta V/V_k)}. \tag{A1}$$

In the simulation, the settling velocities of large bodies are taken to be the rate at which their inclinations are damped by drag. Actually, they would pass back and forth through the central plane, allowing collisions to occur between particles in different levels. This effect is ignored in the present model, which is essentially a "particle in a box" calculation of collisions within each separate level. Neglect of interlevel collisions could cause some underestimate of the surface density in the central plane and the growth rate of bodies there, and overestimate the collisional lifetimes of bodies at other levels. Still, even without this effect the larger bodies are sharply concentrated in the central plane, as seen in Fig. 3. With the surface density used in the present model, the optical thickness due to large bodies is small, meaning that they pass through the central plane with little risk of collision due to such motion (cf. Nakagawa *et al.* 1986).

Using inclination damping instead of actual velocities also underestimates relative velocities associated with vertical oscillations, but this effect is very small. Growth of large bodies occurs in a thin layer with $z/a \sim 10^{-4}$–10^{-5}. Oscillations with such amplitude have velocities of a few to tens of centimeters per second, smaller than the dispersion of radial velocities. This value of dz/dt is used for computing the rate at which the layer of large particles becomes thinner with time due to damping by drag.

APPENDIX B: COLLECTIVE EFFECTS

When the mass loading of particles becomes significant due to settling, the motion of the gas can be affected; i.e., the gas is dragged by the particles at some velocity closer to Keplerian motion than that of the pressure-supported gas. The value of ΔV within the particle-rich layer decreases, and there is shear between the layer and the surrounding gas. Nakagawa *et al.* (1986) derived an expression for the gas velocity in terms of the particle mass loading and response time for particles of a single size. Their solution also assumed laminar motion of the gas. Cuzzi *et al.* (1993) found that their solution was a good approximation to the mean flow in a turbulent particle–gas layer. In my notation, Eq. (2.14) of Nakagawa *et al.* (1986) gives the local deviation of the gas from Keplerian rotation as

$$\Delta V = \left[1 - \left(\frac{\delta}{\rho + \delta}\right)\frac{D^2}{D^2 + \Omega^2}\right]\Delta V_0, \tag{B1}$$

where ρ is the gas density, δ is the space density of particles, $D = (\rho + \delta)/\rho t_e$, and ΔV_0 is the "free stream" value of ΔV in the absence of particles. I generalize their result to a spectrum of particle sizes by assuming the contributions of each size particle can be added, giving

$$\Delta V = \left\{1 - \left(\frac{1}{\rho + \delta}\right)\sum_i \left[\frac{\delta_i D_i^2}{D_i^2 + \Omega^2}\right]\right\}\Delta V_0, \tag{B2}$$

where δ_i is the space density of particles in a size bin, $D_i = (\rho + \delta_i)/\rho t_{ei}$, $\delta = \sum \delta_i$, and the summation is over all size bins. This expression reduces to that of Nakagawa *et al.* for a single particle size. As the size distribution in the layer is usually dominated by a narrow range of sizes, the assumption that effects of different particle populations are additive is adequate. Note that as t_e becomes large for large bodies that are not coupled to the gas, ΔV approaches the free stream value.

In the simulation, ΔV is evaluated for each level within the particle layer; the various levels may have substantially different mass loadings and size distributions. In general, high mass loadings in the central plane are achieved only when the particles are large and poorly coupled to the gas. Thus, ΔV never approaches zero; i.e., the particle layer never achieves Keplerian rotation, no matter how dense it becomes. Note that I do not use the method of Nakagawa *et al.* (1986) to determine particle velocities directly; rather, I find ΔV for the gas, and use its value to solve for particle motions as functions of size as done by Weidenschilling (1977).

APPENDIX C: SHEAR-INDUCED TURBULENCE

As shown by Weidenschilling (1980) and Cuzzi *et al.* (1993), the shear between the particle layer and the surrounding gas is unstable, and will become turbulent. I assume the onset of turbulence occurs when the characteristic Reynolds number of the flow exceeds a critical value. The Reynolds number of the shear flow is

$$\mathrm{Re} = (\Delta V_0 - \Delta V(z))z\rho/\eta, \tag{C1}$$

where η is the viscosity of the gas. I take the critical value to be 100, which is in the middle of the range (45–180) suggested by Cuzzi *et al.* for shear flows.

Turbulence is generated locally by velocity gradients; by symmetry the gradient goes to zero at $z = 0$. Turbulence, however, diffuses from its place of origin, and in the simulation of Cuzzi *et al.* (1993) the central plane is turbulent. I assume that the turbulent eddy velocity at any level (for which $\mathrm{Re} > 100$) is proportional to $\Delta V_0 - \Delta V(z)$, i.e., to the velocity difference, or integral of the velocity gradient, from the particle-free gas.

Global turbulence (e.g., convection) in a rotating system is generally assumed to have a turnover time for the largest eddies equal to the rotation time scale Ω^{-1}; however, for a boundary layer in rotating Ekman shear flow, the eddy time scale is shorter, and can be expressed as $(\mathrm{Ro}\Omega)^{-1}$, where Ro is the Rossby number. Following Cuzzi *et al.* (1993), I assume $\mathrm{Ro} = 80$. This sets the scale of the largest eddies, the turbulence is assumed to have a Kolmogorov spectrum at smaller scales.

APPENDIX D: TURBULENT VELOCITIES AND TRANSPORT

Relative velocities of particles due to turbulence are computed using the model of Völk *et al.* (1978, 1980), modified to account for the fact that the turbulence spectrum has a lower limit to the size of eddies (Weidenschilling 1984). The relative velocities induced by turbulence are added quadratically to the systematic drag-induced velocities between bodies of different sizes.

Turbulence also transports particles between levels. From Völk *et al.*,

the rms velocity of a particle suspended in a turbulent gas with largest eddies having velocity V_t is

$$V_{td} = V_t/(1 + t_e/t_k)^{1/2}, \quad \text{(D1)}$$

where t_k is turnover time scale of the largest eddies. For turbulence produced by shear, I take $t_k = (\mathrm{Ro}\Omega)^{-1}$. In the limit of large bodies $V_{td} \propto t_e^{-1/2}$. The turbulent transport of particles between levels is treated as simple diffusion. The diffusion coefficient in such cases is proportional to the product of the square of the velocity of the diffusing matter times a characteristic time scale, which I take to be t_k.

Bodies that are sufficiently large may have random velocities due to gravitational stirring (Appendix E, below), in addition to motions caused by turbulence. I treat gravitational stirring as "diffusion," but with a different characteristic time scale, $t_0 = \Omega^{-1}$. If the computed rms velocity due to gravitational stirring is taken to be V_g, then the diffusion coefficient is defined as

$$C_D = \frac{\pi}{8}(V_{td}^2 t_k + V_g^2 t_0). \quad \text{(D2)}$$

The diffusive flux between levels i and $(i + 1)$ (mass per unit area per unit time) is taken to be proportional to the concentration gradient:

$$\text{flux}\ (i \rightarrow i+1) = C_D m \left(\frac{N_i}{\rho_i} - \frac{N_{i+1}}{\rho_{i+1}}\right)\left(\frac{\rho_i + \rho_{i+1}}{2\,\Delta z}\right), \quad \text{(D3)}$$

where Δz is the distance between the two levels, and N is the number of particles of mass m per unit volume. If the two levels have different turbulent velocities, the diffusion coefficient is averaged between the levels. The gas densities ρ_i, ρ_{i+1} in the expression ensure that in the limit of small t_e (perfect coupling of particles and gas), if the two levels have different gas densities, diffusion produces a uniform dust/gas ratio rather than a uniform particle concentration. The total mass flux between levels is the sum of the diffusive flux and systematic settling. If the particle size distribution did not change with time, the particle concentration in each level would evolve until a net upward diffusive flux balanced the settling flux.

The diffusion model works well for small particles, but presents problems for large bodies. As mentioned in Appendix A, large bodies are in perturbed Keplerian orbits; their "settling" is actually damping of orbital inclinations rather than a physical velocity. Likewise, "diffusion" between levels is actually due to changes in inclination. Treating this as diffusion can lead to nonphysical results. Note that the "settling velocity" for large bodies [Eq. (A1)] is proportional to t_e^{-1}, while the random velocity induced by turbulence is $\propto t_e^{-1/2}$ when $t_e \gg t_k$. If we ignore gravitational stirring and consider only the effect of turbulence, the settling velocity becomes negligible compared with the turbulent "diffusion" velocity in the limit of large t_e. Modeling the flux of large bodies as diffusion, they are found to diffuse upward (i.e., attain higher inclinations) as they grow larger (t_e increases). This occurs despite the fact that their random velocities decrease with size, and their vertical velocities ($V_k \sin i \simeq V_k z/a$, not settling velocities) become larger than the random velocities that would be excited by turbulence according to Eq. (D1). The model of turbulent stirring by Völk *et al.* assumes that a body is subject only to turbulent drag forces; more careful study is needed for bodies in Keplerian orbits subjected to velocity impulses by turbulent eddies. Such a study, however, is beyond the scope of this paper and not important to its main point. Instead, I suppress this unphysical result by not allowing any upward flux into any level such that $z(=a \sin i) > a\,(V_{td}^2 + V_g^2)^{1/2}/V_k$.

APPENDIX E: GRAVITATIONAL STIRRING

Gravitational stirring is negligible compared with drag unless the bodies are large enough to be in Keplerian orbits. The threshold for stirring is taken to be $t_e\Omega > 2\pi$, i.e., response time greater than the orbital period. Velocities are determined by a balance between stirring by mutual perturbations and damping by drag. Rather than compute an explicit stirring rate, I adopt a simple parameterization of velocities. Numerical models of accreting systems of large planetesimals (Wetherill and Stewart 1993, Weidenschilling *et al.* 1997) tend to show a characteristic velocity distribution: Bodies smaller than the median mass have rather uniform velocities, proportional to the escape velocity of the median bodies. Larger bodies show approximate equipartition of energy, with velocities inversely proportional to the square root of their masses.

As large bodies cross the central plane of the nebula, the effective median mass is determined by a weighted average over all levels that contain large bodies. The median escape velocity is $\overline{V}_e = 2(G\overline{m}/\overline{d})^{1/2}$ where $\overline{m}$,$\overline{d}$ are the mass and diameter of the median-mass body. Velocities are scaled to $\overline{V}_e$ by an assumed Safronov number θ, taken to be 3 in the simulation. This scaling yields gravitational stirring velocity

$$V_g^2 = \overline{V_e^2}(1 - 2\pi/t_e\Omega)/2\theta, \quad \text{(E1)}$$

where the factor $(1 - 2\pi/t_e\Omega)$ is chosen to provide a smooth transition to no stirring at $t_e\Omega = 2\pi$. Equation (E1) applies to bodies smaller than the median size; if $m > \overline{m}$, this expression for V_g^2 is multiplied by $(\overline{m}/m)$ to give equipartition for larger bodies.

APPENDIX F: MECHANICAL PROPERTIES OF PARTICLES

As gravitational instability is not effective, planetesimals/cometesimals must grow by collisional coagulation. It is not reasonable to assume perfect sticking or some arbitrary "sticking efficiency" that is independent of the collisional parameters. Experimental data relevant to such collisions of aggregate bodies are scarce. Therefore, I make the following reasonable assumptions:

At low velocities, small particles adhere by surface forces (van der Waals bonding). The model of Chokshi *et al.* (1993) compares surface forces with energy dissipation to derive a critical sticking velocity that depends on particle sizes, elastic constants, and surface energy. Collisions at less than this velocity result in sticking. Strictly speaking, this model refers to head-on collisions of elastic spheres; however, for simple assumptions about aggregate bodies, the lower contact area is offset by greater dissipation of energy (Weidenschilling and Ruzmaikina 1994). I assume the critical velocity is defined for parameters given by Chokshi *et al.* for water ice.

At impact velocities too large for perfect sticking, other effects may produce coagulation. Irregular shapes may penetrate and interlock. The size dependence of drag-induced velocities results in most impacts being between very unequal bodies, allowing the smaller to become embedded in the larger, perhaps with some material dislodged from the "crater." I assume that each impact adds the mass of the smaller projectile to the larger target. From this combined mass is removed an amount of mass proportional to the energy of the impact measured in the center of mass frame. The excavation coefficient, with nominal value 7×10^{-8} g erg^{-1}, is scaled to an effective impact strength so that the largest "cratering" impact removes 10% of the target's mass; a larger impact shatters the target (Weidenschilling 1984). In both cratering and shattering impacts, fragments are assigned a power-law size distribution and distributed among the smaller size bins.

Small aggregates, with diameters less than 10^{-2} cm, are assumed to have fractal structure with dimension 2.1; hence their densities decrease

with size as $d^{-0.9}$. Bodies larger than 1 cm are assumed to have uniform density of 0.7 g cm^{-3}. The nominal value of impact strength is 10^6 erg g^{-1}. This should not be taken as equivalent to a mechanical strength in tension or compression. Rather, it is a measure of energy absorption in impacts; a porous aggregate is ''lossy'' and dissipates much of the impact energy. In the simulation, the nominal strength does not produce any shattering collisions; bodies of comparable size collide at low relative velocities, and for bodies of disparate size the smaller body does not supply enough energy to shatter the larger.

APPENDIX G: CALCULATION OF OPACITY

In the cool outer portion of the solar nebula opacity is due almost entirely to extinction by solid grains. To estimate optical thickness of the nebula, I use the Rosseland mean extinction coefficient of Pollack *et al.* (1994). At temperatures below 160°K when water ice is condensed, the extinction coefficient is adequately approximated by (cf. their Fig. 6)

$$\kappa = 5(T/160)^2 \text{ cm}^2 \text{ g}^{-1}. \quad \text{(G1)}$$

This value refers to extinction per gram of solar-composition gas, in which the grains are assumed to be smaller than the relevant wavelengths for radiative transfer. In that case, the extinction is proportional to the total mass of particles and is independent of their size distribution. Coagulation and settling produce large particles and change the solids/gas ratio, so the expression for κ must be modified. Assuming a nominal solids/gas ratio of 0.015 for solar composition with refractories and ice condensed, the extinction per gram of solid material is

$$\kappa_S = 333(T/160)^2 \text{ cm}^2 \text{ g}^{-1}. \quad \text{(G2)}$$

I use this value for the mass of solids in particles smaller than the blackbody peak wavelength at the local temperature, $\lambda_{\max} = (0.29/T)$ cm. In the simulation, T is assumed to be 50°K, so $\lambda_{\max} \simeq 60$ μm. Larger particles are assumed to contribute to extinction only in proportion to their total surface area.

ACKNOWLEDGMENTS

I thank D. R. Davis, F. Marzari, and W. K. Hartmann for discussions and comments. This work was supported by NASA Grant NAGW-4149. The Planetary Science Institute is a division of the San Juan Capistrano Research Institute. This is PSI Contribution 340.

REFERENCES

Adachi, I., C. Hayashi, and K. Nakazawa 1976. The gas drag effect on the elliptical motion of a solid body in the primordial solar nebula. *Prog. Theor. Phys.* **56,** 1756–1771.

Asphaug, E., and W. Benz 1996. Size, density, and structure of Comet Shoemaker-Levy 9 inferred from the physics of tidal breakup. *Icarus* **121,** 225–248.

Bailey, M. 1987. The formation of comets in wind-driven shells around protostars. *Icarus* **69,** 70–82.

Biermann, K., and K. W. Michel 1978. On the origin of cometary nuclei in the presolar nebula. *Moon Planets* **18,** 447–464.

Chokshi, A., A. G. G. M. Tielens, and D. Hollenbach 1993. Dust coagulation. *Astrophys. J.* **407,** 806–819.

Cochran, A. L., H. F. Levison, S. A. Stern, and M. J. Duncan 1995. The discovery of Halley-sized Kuiper belt objects using the Hubble Space Telescope. *Astrophys. J.* **455,** 342–346.

Cuzzi, J. N., A. R. Dobrovolskis, and J. M. Champney 1993. Particle-gas dynamics in the midplane of the solar nebula. *Icarus* **106,** 102–134.

Dominik, C., and A. G. G. M. Tielens 1997. The physics of dust coagulation and the structure of dust aggregates in space. *Astrophys. J.,* in press.

Donn, B., and D. Hughes 1986. A fractal model of a cometary nucleus formed by random accretion. In *Proceedings, 20th ESLAB Symposium,* Vol. III, pp. 523–524.

Dubrulle, B., G. Morfill, and M. Sterzik 1995. The dust subdisk in the protoplanetary nebula. *Icarus* **114,** 237–246.

Duncan, M. J., T. Quinn, and S. Tremaine 1988. On the origin of short-period comets. *Astrophys. J.* **328,** L69–L73.

Farinella, P., and D.R. Davis 1996. Short-period comets: Primordial bodies or collisional fragments? *Science* **273,** 938–941.

Fernandez, J. A., and W.-H. Ip 1981. Dynamical evolution of a cometary swarm in the outer planetary region. *Icarus* **47,** 470–479.

Goldreich, P., and W. R. Ward 1973. The formation of planetesimals. *Astrophys. J.* **183,** 1051–1061.

Greenberg, R., S. J. Weidenschilling, C. R. Chapman, and D. R. Davis 1984. From icy planetesimals to outer planets and comets. *Icarus* **59,** 87–113.

Jewitt, D., and J. X. Luu 1995. The Solar System beyond Neptune. *Astron. J.* **109,** 1867–1876.

Jewitt, D., and K. Meech 1988. Optical properties of cometary nuclei and a preliminary comparison with asteroids. *Astrophys. J.* **328,** 974–986.

Kührt, E., and H. U. Keller 1994. The formation of cometary surface crusts. *Icarus* **109,** 121–132.

Larson, H. P., H. Y. Hu, M. Mumma, and H. Weaver 1990. Outbursts of water in Comet P/Halley. *Icarus* **86,** 129–151.

Melosh, H. J., and E. V. Ryan 1997. Asteroids: Shattered but not dispersed. *Icarus,* submitted.

Mizuno, H., W. J. Markiewicz, and H. J. Völk 1988. Grain growth in turbulent protoplanetary accretion disks. *Astron. Astrophys.* **195,** 183–192.

Möhlmann, D. 1996. Cometary activity and nucleus modelling: A new approach. *Planet. Space Sci.* **44,** 541–456.

Mumma, M., P. Weissman, and S. A. Stern 1993. Comets and the origin of the Solar System: Reading the Rosetta stone. In *Protostars and Planets III* (E. Levy and J. Lunine, Eds.), pp. 1177–1252. Univ. of Arizona Press, Tucson.

Nakagawa, Y., K. Nakazawa, and C. Hayashi 1981. Growth and sedimentation of dust grains in the primordial solar nebula. *Icarus* **45,** 517–528.

Nakagawa, Y., M. Sekiya, and C. Hayashi 1986. Settling and growth of dust particles in a laminar phase of a low mass solar nebula. *Icarus* **67,** 375–390.

Pollack, J., D. Hollenbach, S. Beckwith, D. Simonelli, T. Roush, and W. Fong 1994. Composition and radiative properties of grains in molecular clouds and accretion disks. *Astrophys. J.* **421,** 615–639.

Safronov, V. S. 1969. *Evolution of the Protoplanetary Cloud and Formation of the Earth and Planets.* Nauka Press, Moscow. [in Russian] (English translation: NASA TTF-677, 1972.)

Timoshenko, S., and J. N. Goodier 1951. *Theory of Elasticity,* McGraw-Hill, New York.

Völk, H., F. Jones, G. Morfill, and S. Röser 1978. Induced velocities of grains embedded in a turbulent gas. *Moon Planets* **19,** 221–227.

Völk, H., F. Jones, G. Morfill, and S. Röser 1980. Collisions between grains in a turbulent gas. *Astron. Astrophys.* **87,** 316–325.

Weidenschilling, S. J. 1977. Aerodynamics of solid bodies in the solar nebula. *Mon. Not. R. Astron. Soc.* **180,** 57–70.

Weidenschilling, S. J. 1980. Dust to planetesimals: Settling and coagulation in the solar nebula. *Icarus* **44,** 172–189.

Weidenschilling, S. J. 1984. Evolution of grains in a turbulent solar nebula. *Icarus* **60,** 553–557.

Weidenschilling, S. J. 1988. Formation processes and timescales for meteorite parent bodies. In *Meteorites and the Early Solar System* (J. Kerridge and M. S. Matthews, Eds.), pp. 348–371, Univ. of Arizona Press, Tucson.

Weidenschilling, S. J. 1994. Formation of cometary nuclei as "rubble piles." *Nature* **368,** 721–723.

Weidenschilling, S. J. 1995. Can gravitational instability form planetesimals? *Icarus* **116,** 433–435.

Weidenschilling, S. J., and J. N. Cuzzi 1993. Formation of planetesimals in the solar nebula. In *Protostars and Planets III* (E. Levy and J. Lunine, Eds.), pp. 1031–1060. Univ. of Arizona Press, Tucson.

Weidenschilling, S. J., and T. V. Ruzmaikina 1994. Coagulation of grains in static and collapsing protostellar clouds. *Astrophys. J.* **430,** 713–726.

Weidenschilling, S. J., D. Spaute, D. R. Davis, F. Marzari, and K. Ohtsuki 1997. Accretional evolution of a planetesimal swarm. 2. The terrestrial zone. *Icarus,* in press.

Weissman, P. 1985. The origin of comets: Implications for planetary formation. In *Protostars and Planets II* (D. C. Black and M. S. Matthews, Eds.), pp. 895–919. Univ. of Arizona Press, Tucson.

Weissman, P. 1986. Are cometary nuclei primordial rubble piles? *Nature* **320,** 242–244.

Wetherill, G. W., and G. R. Stewart 1993. Formation of planetary embryos: Effects of fragmentation, low relative velocity, and independent variation of eccentricity and inclination. *Icarus* **106,** 190–209.

Whipple, F. L. 1950. A comet model. I. The acceleration of Comet Encke. *Astrophys. J.* **111,** 375–394.

Whipple, F. L. 1972. On certain aerodynamic processes for asteroids and comets. In *From Plasma to Planet* (A. Elvius, Ed.), pp. 211–232. Wiley, New York.

Whitney, C. 1955. Comet outbursts. *Astrophys. J.* **122,** 190–195.

Yamamoto, T., and T. Kozasa 1988. The cometary nucleus as an aggregate of planetesimals. *Icarus* **75**, 540–551.